IEEE Access
Multidisciplinary | Rapid Review | Open Access Journal

Received September 11, 2018, accepted November 3, 2018, date of publication November 6, 2018,
date of current version December 7, 2018.

*Digital Object Identifier 10.1109/ACCESS.2018.2879899*

# Numerical Analysis of a Mid-Water Trawl System With a 6-DOF Otter Board Model and Sea-Trial Verification

**YINGLONG CHEN[1], (Member, IEEE), YEMING YAO[2], ZENGMENG ZHANG[1], AND HUA ZHOU[3]**

[1]Naval Architecture and Ocean Engineering College, Dalian Maritime University, Dalian 116026, China
[2]Nanjing Engineering Institute of Aircraft Systems, Jincheng, AVIC, Nanjing 211100, China
[3]State Key Laboratory of Fluid Power Transmission and Control, Zhejiang University, Hangzhou 310027, China

Corresponding author: Zengmeng Zhang (zzm.zju@163.com)

This work was supported in part by the Fundamental Research Funds for the Central Universities under Grant 017183018, in part by the Doctoral Scientific Research Foundation of Liaoning Province under Grant 201501137, and in part by the National Natural Science Foundation of China under Grant 51475064.

**ABSTRACT** In this paper, we proposed a mathematical model of a mid-water trawl system. The model consisted of towing warps, otter boards, a trawl net, and other rigging components. The warp and the net were modeled with the lumped mass method. The otter board was modeled in 6 degrees of freedom, and the variation in the otter board's hydrodynamic parameters with different yaws, pitches, and roll angles was also considered. We used a first-order approximation to simplify the relationship between the otter board's hydrodynamic parameters and its working angle, and the coefficients included in the otter board model were then estimated using the sea trail data. With this approach, the movement of the otter board was simulated, and its influence on the trawl gear performance was analyzed. The final results of the door depth and the door spread with warp lengths from 200 to 900 m showed good agreements with the sea trail data, and the mean normalized absolute error between the simulation and the measurement was approximately 5%.

**INDEX TERMS** Trawl, otter board, numerical simulation, 6 DOF modeling, hydrodynamic coefficient.

## I. INTRODUCTION

Fish trawling is one of the most important fishing methods in the world. It has accounted for more than 40% of the world's fish catches since the 1950s; thus, it is of great importance to the animal protein supply upon which people depend for a living. A typical trawl system consists of a trawler, warps, otter boards, bridles, a trawl net and other rigging components such as floats and sinkers (Fig.1). The warps connect the trawler and the otter boards, and the upper/lower bridles connect the otter board to the upper/lower wing of the trawl net on each side. The otter board usually provides several optional fastening points for warps and bridles, so it can be adjusted on board to adapt to different fishing conditions. Different fastening points will result in different working angles when the otter boards are towed in the water, thus exerting different hydrodynamic forces on the otter boards and changing the net geometry and position in the water; therefore, it is very important to understand the movement of otter boards during the fishing process to obtain a better prediction of the mid-water trawl system's overall performance.

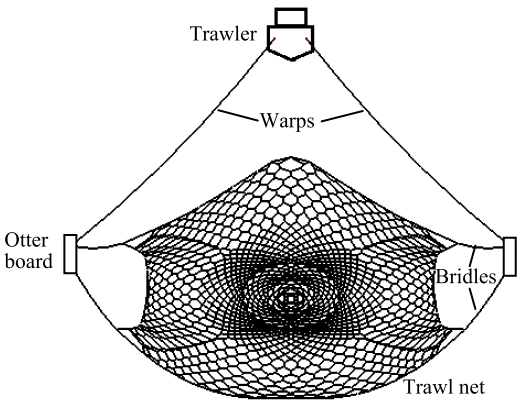


**FIGURE 1.** Schematic representation of trawl system, including trawler, warps, otter bards, bridles and trawl net.

Much research has been done on the dynamic simulation and geometric prediction of trawl systems. Rigid bars were first used to model the submerged supple nets by

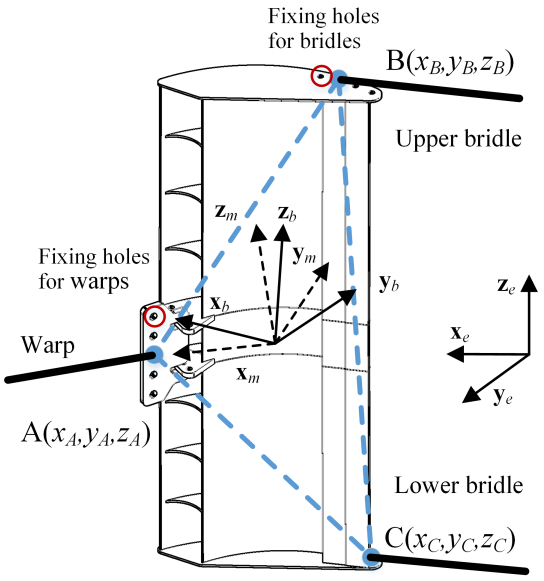


**FIGURE 2.** Otter board model and reference frame definitions. The earth frame, the model frame and the otter board frame of a starboard board are shown in the figure. The blue dashed lines show the structure model of the otter board. The red circles show the fixing holes of warps and bridles.

Bessonneau and Marichal [1], and the dynamics of trawling were successfully predicted. Park [2] used elliptical and exponential functions to model the geometry of a mid-water trawling system and to successfully estimate the gear shape using field data. The attack angle of the otter board was also estimated based on its relationship with the otter board's moment coefficient. A simplified model was established to predict the configuration of a bottom trawl system [3], and the model also provided information on otter boards such as the horizontal spread and the attack angle. Ji *et al*. [4] and Yao *et al*. [5] built a physically based model of a trawl net which was composed of a network of masses and springs, and Sun *et al.* [6] developed a mathematical model of single-boat, mid-water trawl system for training purposes, and in the mathematical model, the trawler was modeled in detail. Furthermore, the tracking control of a mid-water trawl system is very important, and several control strategies were adopted to regulate the trajectory of the trawl net for the target fish shooting [7]–[11], and a nonlinear robust control strategy should be adopted for the control of the trawl system that considers the underwater disturbance and time-delay [12]–[17].

Otter boards are the key components of trawl system; they are used to keep nets horizontally open, and they are also used to obtain a wanted net depth in mid-water trawling. Since they are very important to fishing gear maneuverability as well as fishing efficiency, the design and hydrodynamic analysis of otter boards has become a frequent research topic in recent years. Reite and Sorensen [18] proposed a nonlinear, state-space model of the hydrodynamic force on a multi-foil otter board; the model consists of both steady-state and unsteady hydrodynamic coefficients. Mellibovsky *et al.* [19] conducted a wind tunnel test and obtained six hydrodynamic coefficients of a pelagic otter board, and the test results were compared with flume tank results for the same design. Shen *et al*. [20] investigated the hydrodynamic characteristics of a hyper-lift trawl door using flume experiments. The state-of-art CFD method is also employed in otter board design [21] and optimization [22].

Although the otter board is very important, most of the research dealing with trawl gear simulation did not take its behavior into account. The otter board was usually simplified as a mass point, and its working angle as well as hydrodynamic coefficients were considered as constant during the fishing process [1], [6], [24]. In this paper, we propose a mathematical model of a mid-water trawl system and a full degree of freedom otter board model is included. Linear functions are used to represent the relationship between the otter board's hydrodynamic coefficients and its orientation angles. The coefficients of the linear functions are estimated based on sea trail data. Simulation is conducted to investigate the performance of trawl system considering 6-DOF otter board model, which is then verified through sea trial data.

## II. MATHEMATIC MODEL AND NUMERICAL METHODS

### A. MATHEMATIC MODEL OF AN OTTER BOARD

#### 1) OTTER BOARD MODEL DEFINITION AND REFERENCE FRAMES

In this paper, the warp, bridles and other ropes are connected to the otter board vertexes. Three different frames are used in this paper to sufficiently analyze the otter board's hydrodynamic behavior.

(1) The earth frame. This frame is defined as $\{\mathbf{E}; \mathbf{x}_e, \mathbf{y}_e, \mathbf{z}_e\}$. This is a right-hand frame, and the origin $\mathbf{E}$ can be placed on any point in the horizontal plane; the axes $\mathbf{x}_e$ and $\mathbf{y}_e$ are in the horizontal plane and perpendicular with each other; the axis $\mathbf{z}_e$ is perpendicular to the horizontal plane and opposite to gravity direction. In this reference frame, the interactions between warps, bridles and otter boards are calculated.

(2) The model frames. These frames are defined as $\{\mathbf{O}_m; \mathbf{x}_m, \mathbf{y}_m, \mathbf{z}_m\}$ and $\{\mathbf{O'}_m; \mathbf{x'}_m, \mathbf{y'}_m, \mathbf{z'}_m\}$ for starboard and port otter boards, respectively. These frames are in a mirror relationship, so we only provide the definition of the starboard model frame $\{\mathbf{O}_m; \mathbf{x}_m, \mathbf{y}_m, \mathbf{z}_m\}$. The starboard model frame is a left-hand frame, and the origin $\mathbf{O}_m$ is placed on the otter board's center of gravity; the axes $\mathbf{x}_m$ and $\mathbf{z}_m$ are in the same plane with the otter board model, the axis $\mathbf{x}_m$ points in the direction of the front of the model, the axis $\mathbf{z}_m$ points in the upward direction from the model, and the direction of $\mathbf{y}_m$ can then be ascertained by the left-hand law.

(3) The otter board frames. These frames are defined as $\{\mathbf{O}_b; \mathbf{x}_b, \mathbf{y}_b, \mathbf{z}_b\}$ and $\{\mathbf{O'}_b; \mathbf{x'}_b, \mathbf{y'}_b, \mathbf{z'}_b\}$. Similar to the model frames, these two frames are also in a mirror relationship, and here, we only define the starboard otter board frame $\{\mathbf{O}_b; \mathbf{x}_b, \mathbf{y}_b, \mathbf{z}_b\}$. The origin $\mathbf{O}_b$ is placed on the same point as $\mathbf{O}_m$, the axes $\mathbf{x}_b$, and $\mathbf{z}_b$ are in the flat surface of the otter board, the axis $\mathbf{x}_b$ points in the direction of the front of the otter

board, and the axis $\mathbf{z}_b$ points in the upward direction from the otter board. The direction of $\mathbf{y}_b$ can then be ascertained by the left-hand law.

### 2) OTTER BOARD ORIENTATION ANGLES

The otter board's orientation angles can be calculated using the relative water velocity in the otter board frames:

$$\alpha = \arcsin \frac{u^{wb}_{b,y}}{\sqrt{(u^{wb}_{b,x})^2 + (u^{wb}_{b,y})^2}} \tag{1}$$

$$\beta = \arcsin \frac{u^{wb}_{b,z}}{\sqrt{(u^{wb}_{b,x})^2 + (u^{wb}_{b,z})^2}} \tag{2}$$

where $\alpha$ and $\beta$ are the attack angle and slip angle, respectively. The superscript denotes the relative velocity of water ($w$) in relation to the otter board ($b$), and the subscripts denote the reference frame and the axis.

The relative velocity of water in relation to the otter board in the otter board frame can be represented as follows:

$$u^{wb}_{b,x} = \mathbf{u}^{wb}_e \cdot \mathbf{n}^{b,x}_e, \quad u^{wb}_{b,y} = \mathbf{u}^{wb}_e \cdot \mathbf{n}^{b,y}_e, \quad u^{wb}_{b,z} = \mathbf{u}^{wb}_e \cdot \mathbf{n}^{b,z}_e \tag{3}$$

where $\mathbf{n}^{b,i}_e$ is the direction vector of axis $i$ of the trawl door frame in the earth frame; $\mathbf{u}^{wb}_e$ is the relative velocity vector of water in relation to the otter board in the earth frame, which can be given by:

$$\mathbf{u}^{wb}_e = \mathbf{u}^{we}_e - \frac{1}{3}(\mathbf{u}^{Ae}_e + \mathbf{u}^{Be}_e + \mathbf{u}^{Ce}_e) \tag{4}$$

The relation between the otter board frame and the model frame can be described by a transformation matrix with Tait-Bryan angles [19]:

$$\mathbf{R}^b_m = \begin{bmatrix} c_\varphi c_\theta & c_\varphi s_\theta s_\psi - c_\psi s_\varphi & s_\varphi s_\psi + c_\psi c_\varphi s_\theta \\ c_\theta s_\varphi & c_\varphi c_\psi + s_\varphi s_\theta s_\psi & c_\psi s_\varphi s_\theta - c_\varphi s_\psi \\ -s_\theta & c_\theta s_\psi & c_\theta c_\psi \end{bmatrix} \tag{5}$$

In the transformation matrix, $s$ and $c$ represent sine and cosine, respectively, and $\varphi, \theta$ and $\psi$ are the yaw, pitch and roll angle, respectively. It is notable that the Tait-Bryan angles of the starboard and port frames are different, and their relationship can be written as:

$$\varphi_r = -\varphi_l, \quad \theta_r = \theta_l, \quad \psi_r = -\psi_l \tag{6}$$

The subscript of the Tait-Bryan angle denotes whether it is in a starboard frame ($r$) or a port frame ($l$).

The axes direction vectors of the model frames in the earth frame can be derived as follows:

$$\mathbf{n}^{m,z}_e = \mathbf{l}_{BC} / |\mathbf{l}_{BC}| \tag{7}$$

$$\mathbf{n}^{m,y}_e = k_d \frac{\mathbf{l}_{AC} \times \mathbf{l}_{BC}}{|\mathbf{l}_{AC} \times \mathbf{l}_{BC}|} \tag{8}$$

$$\mathbf{n}^{m,x}_e = k_d \cdot \mathbf{n}^{m,z}_e \times \mathbf{n}^{m,y}_e \tag{9}$$

where $k_\mathrm{d} = 1$ when used in a starboard frame, and $k_\mathrm{d} = -1$ when used in a port frame; $\mathbf{l}_\mathrm{AC}$ and $\mathbf{l}_\mathrm{BC}$ are the length vectors

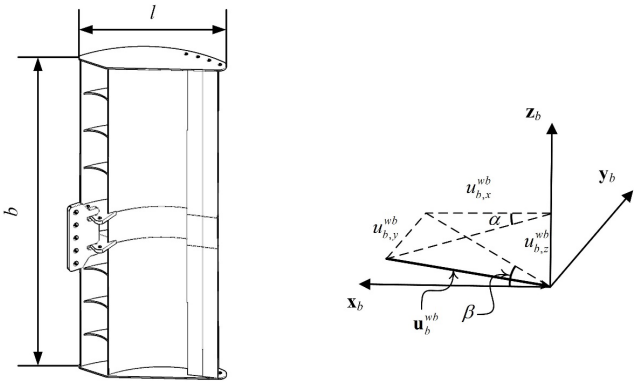


**FIGURE 3.** The definitions of the otter board parameters, $b$ is defined as the span of the otter board, $l$ is defined as the chord length, and $\alpha$ and $\beta$ are defined as the attack angle and the slip angle, respectively.

of the otter board model's edges, and they can be represented by the spatial coordinates of the otter board model's vertexes in the earth frame, for example:

$$\mathbf{l}_{AC} = [x_A - x_C, y_A - y_C, z_A - z_C]^\mathrm{T} \tag{10}$$

The axes direction vectors of the otter board frames in the earth frame can then be calculated by the axes direction vectors of the model frames and the transformation matrix:

$$\mathbf{n}^{b,x}_e = \mathbf{R}^b_m \cdot \mathbf{n}^{m,x}_e, \quad \mathbf{n}^{b,y}_e = \mathbf{R}^b_m \cdot \mathbf{n}^{m,y}_e, \quad \mathbf{n}^{b,z}_e = \mathbf{R}^b_m \cdot \mathbf{n}^{m,z}_e \tag{11}$$

Substituting Eq. (4) and Eq. (11) into Eq. (3), we obtain the relative velocity of the water in relation to the otter board in the otter board frame, following which the otter board orientation angles can be calculated by Eq. (1) and Eq. (2).

### 3) HYDRODYNAMIC FORCES AND THE MOMENT OF THE OTTER BOARD

Six hydrodynamic coefficients are used to describe the forces and moments exerted on the otter board in the otter board frames:

$$\begin{aligned} F_i &= C^F_i \cdot \rho \cdot S_o \cdot u^2/2 \\ M_i &= C^M_i \cdot \rho \cdot S_o \cdot u^2 \cdot d_i/2 \quad (i = x, y, z) \end{aligned} \tag{12}$$

where $C^F_i$ and $C^M_i$ are hydrodynamic and moment coefficients, $\rho$ is the fluid density, $S_\mathrm{o}$ is the project area of the otter board, and $u$ is the relative water velocity. $d_\mathrm{i}$ is the relevant lever length of the moment components, which can be represented by the span $b$ and chord length $l$ of the otter board (Fig. 3):

$$d_x = b, \quad d_y = \sqrt{b^2 + l^2}, \quad d_z = l \tag{13}$$

The six hydrodynamic coefficients of the otter board are in complicated relationships with the otter board orientation angles. In this article, we simplified them into a linear relationship with the attack angle or the slip angle based on the

experimental results by [18], [19]:

$$\begin{bmatrix} C_x^F \\ C_y^F \\ C_z^F \\ C_x^M \\ C_y^M \\ C_z^M \end{bmatrix} = \begin{bmatrix} a_1 & 0 \\ a_2 & 0 \\ 0 & b_3 \\ a_4 & 0 \\ 0 & b_5 \\ a_6 & 0 \end{bmatrix} \cdot \begin{bmatrix} \alpha \\ \beta \end{bmatrix} + \begin{bmatrix} c_1 \\ c_2 \\ c_3 \\ c_4 \\ c_5 \\ c_6 \end{bmatrix} \tag{14}$$

where $a_i$, $b_i$ and $c_i$ are constant parameters which can be determined by experiments.

#### 4) DYNAMICS OF THE OTTER BOARD

In the dynamics analysis of the otter board, we neglected the Coriolis force because of the low speed of the trawl system. The otter board equation of motion can be given as

$$\mathbf{M}_b \cdot \dot{\nu}_b = \tau_b \tag{15}$$

where $\nu_\mathrm{b} = [u, v, w, p, q, r]^\mathrm{T}$ is the linear and angular velocity of the otter board in the otter board frame, and $\tau_\mathrm{b} = [X, Y, Z, K, M, N]^\mathrm{T}$ is the total external force and moment exerted on the otter board; $\boldsymbol{M}_\mathrm{b}$ is the inertia matrix of the otter board, and because we placed $\boldsymbol{O}_\mathbf{m}$ on the otter board model's center of gravity, $\boldsymbol{M}_\mathrm{b}$ can be specified as:

$$\begin{aligned} \mathbf{M}_b &= \begin{bmatrix} m_{ob}\mathbf{I}_{3\times3} & \mathbf{0}_{3\times3} \\ \mathbf{0}_{3\times3} & \mathbf{I}_d \end{bmatrix} \\ &= \begin{bmatrix} m_{ob} & 0 & 0 & & & \\ 0 & m_{ob} & 0 & & \mathbf{0}_{3\times3} & \\ 0 & 0 & m_{ob} & & & \\ & & & I_x & -I_{xy} & -I_{xz} \\ & \mathbf{0}_{3\times3} & & -I_{yx} & I_y & -I_{yz} \\ & & & -I_{zx} & -I_{zx} & -I_z \end{bmatrix} \end{aligned} \tag{16}$$

where $m_{ob}$ is the mass of the otter board; $I_\mathrm{x}$, $I_\mathrm{y}$ and $I_\mathrm{z}$ are the moments of inertia about $\mathbf{x}_\mathrm{b}$, $\mathbf{y}_\mathrm{b}$ and $\mathbf{z}_\mathrm{b}$; $I_\mathrm{xy}$, $I_\mathrm{yx}$, $I_\mathrm{xz}$, $I_\mathrm{zx}$, $I_\mathrm{yz}$ and $I_\mathrm{zy}$ are the products of inertia and $I_\mathrm{xy} = I_\mathrm{yx}$, $I_\mathrm{xz} = I_\mathrm{zx}$, $I_\mathrm{yz} = I_\mathrm{zy}$.

The external force $\boldsymbol{\tau}_\mathrm{b}$ exerted on the otter board contains the hydrodynamic force $\boldsymbol{\tau}_\mathrm{b}^\mathrm{h}$, the tension force of the warp and bridles $\boldsymbol{\tau}_\mathrm{b}^\mathrm{l}$, and the gravity and buoyancy $\boldsymbol{\tau}_\mathrm{b}^\mathrm{GB}$. The generalized force from the warp and bridles can be given as:

$$\begin{aligned} \tau_b^l = &\begin{bmatrix} \mathbf{R}_e^b \mathbf{f}_e^{wp} \\ \mathbf{P}_b^{wp} \times (\mathbf{R}_e^b \mathbf{f}_e^{wp}) \end{bmatrix} + \begin{bmatrix} \mathbf{R}_e^b \mathbf{f}_e^{lb} \\ \mathbf{P}_b^{lb} \times (\mathbf{R}_e^b \mathbf{f}_e^{lb}) \end{bmatrix} \\ &+ \begin{bmatrix} \mathbf{R}_e^b \mathbf{f}_e^{ub} \\ \mathbf{P}_b^{ub} \times (\mathbf{R}_e^b \mathbf{f}_e^{ub}) \end{bmatrix} \end{aligned} \tag{17}$$

where $\mathbf{P}_b$ is the position vector of the fastening point of the warp or bridles in the otter board frame, $\mathbf{f}_e$ is the tension force vector of the warp or bridles in the earth frame, and the superscripts of $\mathbf{P}_b$ and $\mathbf{f}_e$ denote the warp ($w_p$), lower bridle ($l_b$) and upper bridle ($u_b$); $\mathbf{R}_e^b$ is the transformation matrix from the earth frame to the otter board frame, and it can be represented by the axes direction vectors of the model frames which are calculated by Eq. (11):

$$\mathbf{R}_e^b = \begin{bmatrix} \mathbf{n}_e^{b,x} & \mathbf{n}_e^{b,y} & \mathbf{n}_e^{b,z} \end{bmatrix}^\mathrm{T} \tag{18}$$

The generalized force from gravity and buoyancy can be written as

$$\tau_b^{GB} = \begin{bmatrix} (m_{ob} - V_{ob}\rho)\mathbf{R}_e^b \mathbf{g}_e \\ \mathbf{0}_{3\times1} \end{bmatrix} \tag{19}$$

where $V_{ob}$ is the volume of the otter board; and $\rho$ is the fluid density; and $\mathbf{g}_e$ is the gravity vector in the earth frame. Because we put the origin of the otter board frame on the center of gravity, the gravity and buoyancy will not induce any moment.

### B. MATHEMATIC MODEL OF THE TRAWL

There are various methods for modeling the trawl net, including the lumped mass method, the rigid bar method and the finite element method. In this paper, the lumped mass method was adopted to describe the dynamics of the trawl net. The trawl net was first discretized into a large number of units according to the trawl mesh structure, and each discrete element was simplified as a mass-spring-damper model. A trawl knot can be regarded as a sphere element with mass, and the trawl mesh bar can be assumed to be a spring element with mass distributed on the trawl knot.

#### 1) TENSION FORCES ON THE ROPES

Tension force $\mathbf{T}$ acting on the trawl mesh bar is composed of the elastic force $\mathbf{T}_e$ and the damping force $\mathbf{T}_c$. $\mathbf{T}_e$ is assumed to be a zero force when the actual length is less than the initial length; $\mathbf{T}_c$ changes proportionally with the length's expansion rate. These forces can be written as:

$$\mathbf{T}_\mathrm{e} = \begin{cases} -EA \cdot \dfrac{|\mathbf{r}| - l_0}{l_0} \cdot \dfrac{\mathbf{r}}{|\mathbf{r}|} & |\mathbf{r}| > l_0 \\ 0 & |\mathbf{r}| \le l_0 \end{cases} \tag{20}$$

$$\mathbf{T}_\mathrm{c} = -c_l \cdot \frac{\mathbf{r} \cdot \Delta\mathbf{v}}{|\mathbf{r}|} \cdot \frac{\mathbf{r}}{|\mathbf{r}|} \tag{21}$$

where $E$ and $A$ are the modulus and cross-sectional area of the ropes, respectively; $l_0$ is the initial length of the ropes; $\mathbf{r}$ is the length vector along the mesh bar; $c_l$ is the inner damping coefficient of the ropes; and $\Delta\mathbf{v}$ is the relative velocity vector between the two ends of a rope.

#### 2) HYDRODYNAMIC FORCES ON TRAWL KNOTS

The trawl knot can be assumed to be a sphere, and the hydrodynamic force on the knots can be given by:

$$\mathbf{H}_k = -\frac{1}{2} C_D \rho S_k \mathbf{v}^2 \cdot \frac{\mathbf{v}}{|\mathbf{v}|} \tag{22}$$

where $C_D$ is the drag coefficient of the knot, $S_\mathrm{k}$ is the project area of the knot, and $\mathbf{v}$ is the relative velocity vector.

#### 3) HYDRODYNAMICS ON TRAWL MESH BARS

The hydrodynamic force on a rope can be divided into the drag force $\mathbf{F}_p$ and the viscous force $\mathbf{F}_f$. $\mathbf{F}_p$ is located in the plane composed of $\mathbf{u}_{mw}$ and the rope's direction, while $\mathbf{F}_f$ is along the rope's direction and has an angle with the

velocity vector $\mathbf{u}_{mw}$. The hydrodynamic forces $\mathbf{F}_p$ and $\mathbf{F}_f$ can be expressed as [23]:

$$\mathbf{F}_{\mathrm{P}} = C_{N90} \cdot \frac{\rho(\mathbf{u} \cdot \sin\alpha)^2}{2} \cdot S_N \cdot \mathbf{n}_{\mathrm{P}} \tag{23}$$

$$\mathbf{F}_{\mathrm{f}} = C_f \cdot \frac{\rho(\mathbf{u} \cdot \cos\alpha)^2}{2} \cdot S_f \cdot \mathbf{n}_{\mathrm{f}} \tag{24}$$

where $C_{N90}$ is the resistance coefficient; $C_f$ is the viscous friction coefficient; $\alpha$ is the attack angle of the mesh bar; $S_N$ and $S_f$ are the project area and the wet area of the cylinder, respectively, with $S_N = dl, S_f = \pi dl$; $d$ and $l$ are the diameter and length of the rope. $\mathbf{n}_p$ and $\mathbf{n}_f$ are the direction vectors of $\mathbf{F}_p$ and $\mathbf{F}_f$.

#### 4) DYNAMIC EQUATION

According to an analysis of the forces acting on the trawl net, the dynamic formula can be expressed as:

$$(m + \Delta m)\mathbf{a} = \mathbf{T} + \mathbf{H} + \mathbf{W} \tag{25}$$

where $\mathbf{a}$, $\mathbf{m}$, and $\Delta\mathbf{m}$ are acceleration vector, real mass and added mass of the trawl net elements such as knots, mesh bars and ropes. $\mathbf{T}$, $\mathbf{H}$ and $\mathbf{W}$ are the rope tension, the hydrodynamic force and the weight in water, respectively.

The added mass of the mesh bar can be obtained by:

$$\Delta m_r = \begin{bmatrix} \rho C_{mt} V_r & 0 & 0 \\ 0 & \rho C_{mn} V_r & 0 \\ 0 & 0 & \rho C_{mb} V_r \end{bmatrix} \tag{26}$$

where $C_{mt}$, $C_{mn}$ and $C_{mb}$ are the added mass coefficients in the direction of $t$, $n$ and $b$, respectively. $V_r$ is the volume of the mass points.

The added mass of the trawl knot unit can be written as:

$$\Delta m_k = \rho C_m V_k \tag{27}$$

where $V_k$ is the volume of the knot, and $C_{\mathrm{m}}$ is the added mass coefficient. The weight in fluid of the unit can be given by:

$$\mathbf{W} = (m - \rho V)\,\mathbf{g} \tag{28}$$

where $\mathbf{g}$ is the gravity acceleration vector, and $V$ is the volume of the components including knots, warps and mesh bars.

### C. MATHEMATIC MODEL OF A CANVAS KITE

#### 1) DYNAMIC EQUATION

Canvas is a flexible spreading device to maintain the vertical opening of the trawl mouth that can provide a larger lift force and less weight compared with the floaters. For simplification, this paper only considers the spatial translation and pitching motion of the canvas, and the dynamic equation for the canvas kite can be given by:

$$(m_c + \Delta m_c)\,\mathbf{a}_c = \mathbf{T}_{\mathrm{c}} + \mathbf{W}_c + \mathbf{H}_{\mathrm{c}} \tag{29}$$

where $m_{\mathrm{o}}$ is the mass of the canvas, $\Delta m_{\mathrm{o}}$ is the added mass, $\mathbf{a_c}$ is the acceleration vector, $\mathbf{T}_{\mathrm{c}}$ is the tension forces of the ropes acting on the canvas, $\mathbf{W}_{\mathrm{c}}$ is the weightless buoyancy of the canvas, and $\mathbf{H}_{\mathrm{c}}$ is the force exerted on the canvas by the fluid.

#### 2) FORCES ACTING ON THE CANVAS

As the rotary inertia of flexible canvas is quite small, we assume the attack angle of the canvas is decided by the positions of the connecting mesh bars. The hydrodynamic forces acting on the canvas can be obtained by the following equations [24]:

$$\begin{aligned} \mathbf{H}_{cL} &= -\rho S_c C_{cL}(a_c)\,\mathbf{u}^2 \cdot \mathbf{n}_g/2 \\ \mathbf{H}_{cD} &= -\rho S_c C_{cD}(a_c)\,|\mathbf{u}| \cdot \mathbf{u}/2 \end{aligned} \tag{30}$$

where $\rho$ is the fluid density; $S_c$ is the area of the canvas kite; $\mathbf{u}$ is the current velocity vector; $\mathbf{n}_g$ is gravity direction vector;$C_{cL}(a_{\mathrm{c}})$ and $C_{cD}(a_{\mathrm{c}})$ are the lift and drag coefficients of the canvas; $a_{\mathrm{c}}$ is the attack angle with $a_c = \beta_{\mathrm{c}}\eta_{\mathrm{c}}$; and $\beta_{\mathrm{c}}$ is the pitching angle, which is determined by the outline and the installation rope. The pitching angle $\beta_{\mathrm{c}}$ can be written as:

$$\beta_c = \arctan\frac{(x_i - x_j)}{(y_i - y_j)} \tag{31}$$

where $x_i$ and $x_j$ are the $x$-direction coordinates of the mesh mass elements connected by the lifting canvas, and $y_i$ and $y_j$ are the y-direction coordinates of the mesh mass elements connected by the lifting canvas. The motion angle $\eta_{\mathrm{c}}$ of the canvas can be written as:

$$\eta_c = \arctan\frac{v_{cx}}{v_{cy}} \tag{32}$$

where $v_{cx}$ and $v_{cx}$ are the canvas speeds in the $x$ and $y$ directions, respectively.

The tension forces $\mathbf{T}_{\mathrm{c}}$ acting on the canvas kite is the resultant force of the rope acting on the canvas, which can be obtained by Eq. (20) $\sim$ Eq. (21).

The weight in fluid of the canvas kite is as follows:

$$\mathbf{W}_c = (m_c - \rho v_c)\,\mathbf{g} \tag{33}$$

where $m_{\mathrm{c}}$ and $v_{\mathrm{c}}$ are the mass and volume of the canvas, respectively, and $\mathbf{g}$ is the gravity acceleration vector.

## III. PARAMETER ESTIMATION OF THE OTTER BOARD

### A. DESCRIPTION OF THE PARAMETER ESTIMATION

Otter boards are spatially curved structures with complex shapes, and the hydrodynamic coefficients are difficult to derive theoretically. Therefore, the hydrodynamic characteristics of the otter board are generally analyzed using the CFD method [22], [25]–[27] and the experimental method [18], [19]. However, both methods derive the hydrodynamic (moment) coefficient of the otter board by directly measuring the force acting on the otter board. Obviously, although the two methods are accurate and direct, they also have the disadvantages of large workloads and complicated data processing. Therefore, these two methods are primarily used for the design and optimization of the otter board. For the otter boards that have been put into practical ship applications, it is unrealistic to use these two methods to determine the hydrodynamic coefficients.

As mentioned above, the otter board is an important component of the trawl system, and its hydrodynamic characteristics directly determine the position and attitude of the net under water. Therefore, based on the sea test results of the net tool, the 6-DOF hydrodynamic (moment) coefficients of the otter board are determined by the parameter identification method. The calculation results are compared with previous experimental results, and the rationality of the otter board model and its parameter identification is demonstrated.

### B. PARAMETER ESTIMATION ALGORITHM

The parameter identification problem for an otter board can be equivalently converted into an optimization problem:

$$\begin{aligned} &\min\ f(\mathbf{x}),\\ &\text{s.t. } \mathbf{x}^{\min} \le \mathbf{x} \le \mathbf{x}^{\max} \end{aligned} \tag{34}$$

where $f(\mathbf{x})$ is the objective function. The optimization goal in this paper is that the sum of the absolute values of the deviation between the simulated data and the test data at different warp lengths and towed speeds is a minimum; therefore, $f(\boldsymbol{x})$ can be written as:

$$\begin{aligned} f(\mathbf{x}) = \sum_{i=1}^{15} (&\lambda_{DS} \left| Ds^i_{\text{sim}} - Ds^i_{\text{exp}} \right| + \lambda_{Dd} \left| Dd^i_{\text{sim}} - Dd^i_{\text{exp}} \right| \\ &+ \lambda_{Wt} \left| Wt^i_{\text{sim}} - Wt^i_{\text{exp}} \right| + \lambda_{Nd} \left| Nd^i_{\text{sim}} - Nd^i_{\text{exp}} \right|) \end{aligned} \tag{35}$$

where $D$s, $D$d, $W$t, and $N$d represent the horizontal expansion of the otter board, the depth of the otter board, the tension of the otter board and the depth data of the mesh, respectively, the subscripts indicate the experimental value (*exp*) or the simulated value (*sim*), and the superscripts indicate the data group. Since the variation range of each simulation result is different, the absolute value of the deviation between each simulation and test result is multiplied by a weighting coefficient $\lambda$, $\lambda \in (0, 1)$, which is used to adjust each simulation result to the otter board; this value is the parameter identification effect.

In Eq. (34), $\mathbf{x}$ is an optimization parameter vector; the primary unknown parameters in the mesh model of this paper are the six hydrodynamic (moment) coefficients of the otter board. According to the results of [18] and [19], each hydrodynamic (moment) coefficient can be approximated as a linear function of the otter board attack angle $\alpha$ or the slip angle $\beta$, as is shown in Eq. (37). Therefore, in this paper, we select the coefficients of the six hydrodynamic (moment) coefficient fitting functions of the otter board as the variables to be identified; that is, $\mathbf{x}$ can be expressed as:

$$\mathbf{x} = (a_1, c_1, a_2, c_2, b_3, c_3, a_4, c_4, b_5, c_5, a_6, c_6)^{\mathrm{T}} \tag{36}$$

Given a set of initial values of the parameters of the otter board to be identified, by simulating the net model, the deviation between the simulated steady state and the experimental results is obtained, and the optimized objective function value can be calculated by Eq. (35). By changing the value of the otter board parameter vector $\mathbf{x}$ by a certain law, comparing the objective function values under the different $\mathbf{x}$, and continuously optimizing $\mathbf{x}$ to minimize the objective function value, the identification result of the otter board parameters can be obtained.

## IV. RESULTS AND DISCUSSION

### A. EXPERIMENTAL SETUP

A sea-trial verification was conducted to verify the accuracy of the proposed mathematical model of the trawl system in the Southwest Pacific Ocean [28]. The field test was conducted on a Chinese fishing vessel called "*Kaifuhao*" (7685GT), which is 105 m in length and 20 m in width. The trawl net investigated in this paper is a hexagonal type net produced by *Tornet* of Iceland. The gear is 496.5 m in length and 1632 m in circumference. The number of net mouth meshes is 68, and the size of net mouth meshes is 24 m. The large meshes are made of *Dyneema* ropes, and the trawl bag is a polyamide (PA) material. The head and foot ropes are both 387 m in length, and the sinkers mounted on the foot rope are chain with a diameter of 16 mm. A flexible canvas kite is used instead of the floaters for the gear that is mounted on the center of headrope, and it has an effective area of 6.75 $m^2$. A rectangular otter board with an area of 12 $m^2$ is adopted on the trawler, and the weight in water is approximately 22 kN. The weight of the clump mounted on the wings is 12 kN. The diameter of the warps is 32 mm, and the warp weight in water per meter is approximately 28 N. A rectangular otter board is used on the trawler, and the main parameters of otter board can be seen in Table 1.

Using the instruments mounted on the ship, it is possible to obtain some parameters of the trawl system. To observe the states of the trawl winch, measurements of the warp length $l_{\text{w}}$ and tension $T_{\text{w}}$ are taken with the transducers mounted on the trawl winch and recorded automatically on a computer. Trawl sonar is used to measure the vertical position of the trawl net, height and horizontal spread of the trawl mouth. The sonar is mounted at the center of the headrope, and the image of the trawl mouth can be recorded. Auto pilot is used for the automatic control of the heading course through the manipulation of the rudder. The Autotrawl system developed by *Scantrol* is adopted for the control of the warps through the automatic adjustment of the trawl winches. For catching the fish schools, color scanning sonar and an echo sounder are used to obtain the position information of the targeted fish horizontally and vertically, respectively.

### B. PARAMETER ESTIMATION RESULTS

The parameter estimation results of $a_1 \sim c_6$ can be seen in bellow:

$$\begin{bmatrix} C_x^F \\ C_y^F \\ C_z^F \\ C_x^M \\ C_y^M \\ C_z^M \end{bmatrix} = \begin{bmatrix} 1.19 & 0 \\ 2.47 & 0 \\ 0 & -0.3 \\ -0.46 & 0 \\ 0 & 0.24 \\ 0.92 & 0 \end{bmatrix} \cdot \begin{bmatrix} \alpha \\ \beta \end{bmatrix} + \begin{bmatrix} 0.041 \\ 0.67 \\ 0.01 \\ 0.02 \\ 0.016 \\ 0.25 \end{bmatrix} \tag{37}$$

**TABLE 1. Otter board parameters.**

| Parameter | Definition | Value |
|---|---|---|
| $I_x$ /$kgm^2$ | moments of inertia about $\mathbf{x}_b$ | 7528 |
| $I_y$/$kgm^2$ | moments of inertia about $\mathbf{y}_b$ | 8489 |
| $I_z$/$kgm^2$ | moments of inertia about $\mathbf{z}_b$ | 1143 |
| $I_{xy}$ /$kgm^2$ | products of inertia | 56.3 |
| $I_{xz}$/$kgm^2$ | products of inertia | 0 |
| $I_{yz}$/$kgm^2$ | products of inertia | 0 |
| $\varphi$/° | Tait-Bryan yaw angle | 7.2 |
| $\theta$/° | Tait-Bryan pitch angle | 19.1 |
| $\psi$/° | Tait-Bryan roll angle | 18.2 |
| $V_{ob}$/$m^3$ | volume of otter board | 0.33 |
| $l$/$m$ | chord length | 2.13 |
| $b$/$m$ | span of otter board | 5.63 |
| $S$/$m$ | project area of otter board | 12 |
| $m_{ob}$/kg | mass of otter board | 2600 |

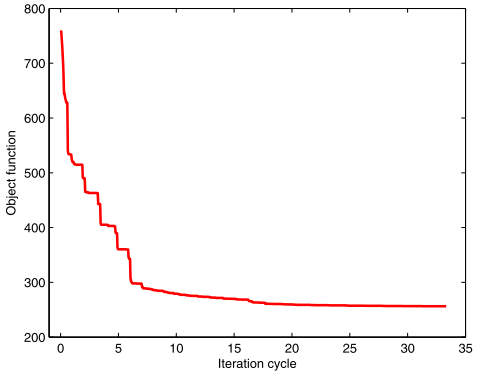


**FIGURE 4. This figure shows the curve of the parameter estimation object function with the iteration cycle.**

Fig. 4 shows the variation curve of the objective function value during the parameter identification iterations. The abscissa is the iteration period, and the parameters of $a_1$ to $c_6$ are all calculated as one iteration period. It can be seen from the figure that through the parameter iteration, the value of the objective function becomes approximately 1/3 of the first, indicating that the estimation parameters of the otter board are more consistent with the sea test data than the initial values, and the validity of the parameter identification algorithm designed in this paper is verified.

It can also be seen from Fig. 4 that the objective function value decreases rapidly in the initial stage of the parameter identification, and the whole changes in the form of a negative exponential function. In the calculation process, especially in the initial stage of calculation, the objective function value shows a relatively obvious step form change, which is primarily due to the inconsistent influence of the parameters of the otter board hydrodynamic coefficient functions participating in the iteration of the objective function.

The lift coefficient $C_l$ and the drag coefficient $C_d$ are the two most important hydrodynamic coefficients of the otter board. Fig. 5 shows the lift and drag coefficients identified by

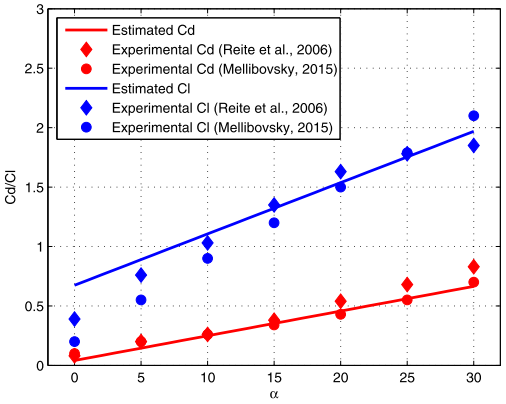


**FIGURE 5. This figure shows the comparison of parameter estimation results with the sea-trial; the blue solid line represents the estimated lift coefficient $C_l$, and the red solid line represents the estimated drag coefficient $C_d$.**

the sea trial data in this paper compared with the otter board model test data of [18] and [19]. It can be seen that the lift and drag coefficients of the otter board and the hydrodynamic coefficients obtained by the otter board test are consistent within the range of $0 \sim 30°$ of the otter board angle. The lift and drag coefficients of the otter board are all increasing functions of the angle of attack. However, the maximum deviation of the drag coefficient appears when the angle of attack $\alpha$ is approximately 30°, and the maximum deviation is approximately 0.1. The lift coefficient is larger when the angle of attack is small, but the slope of the lift coefficient relative to the angle of attack is smaller than the model test result. The otter board lift coefficient is in good agreement with the experimental data in the attack angle range of $15 \sim 30°$, and the maximum deviation is also approximately 0.1. Since the underwater current disturbance on the otter board is difficult to observe, this may lead to deviation in parameter identification.

### C. TRAWL SYSTEM SIMULATION RESULTS

#### 1) OTTER BOARD'S WORKING ANGLE INFLUENCE

Fig. 6 shows the curve of the working angle of the otter board as a function of the warp length. In the figure, $\delta$ is the inclination angle of the otter board which can be defined as:

$$\delta = \arccos\left(\frac{z_e^{b,z}}{\left|\mathbf{n}_e^{b,z}\right|}\right)$$
$$\mathbf{n}_e^{b,z} = [x_e^{b,z}, y_e^{b,z}, z_e^{b,z}] \tag{38}$$

where $\mathbf{n}_e^{b,z}$ is the direction vector of the $\mathbf{z}_b$ axis of the otter board coordinate system in the ship coordinate system, and $x_e^{b,z}$, $y_e^{b,z}$, $z_e^{b,z}$ is the component in the direction of the ship coordinate system $\mathbf{x}_e$, $\mathbf{y}_e$, $\mathbf{z}_e$ axis.

#### 2) OTTER BOARD'S INSTALLATION ANGLE INFLUENCE

To assist the user in adjusting the performance of the otter board, a plurality of holes is located on the otter board for fixing the warp and the hand rope. When the warp and the

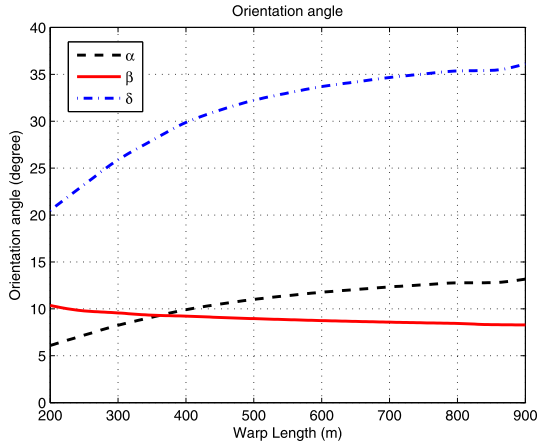


**FIGURE 6.** This figure shows the orientation angle results of the otter board with the warp length; the blue dashed and black dotted lines represent the attack angle $\alpha$ and the slip angle $\beta$, respectively, and the red solid line represents the attack inclination angle $\delta$.

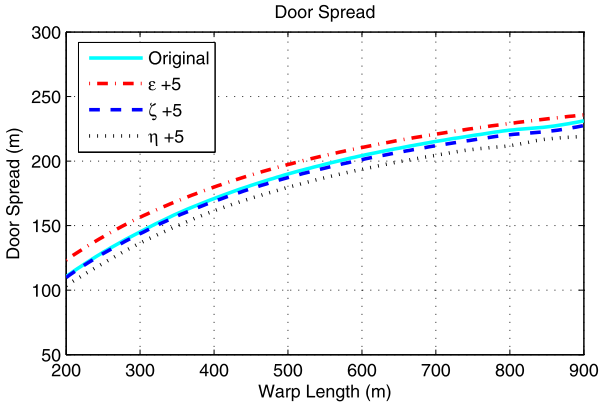


**FIGURE 7.** This figure shows the spread expansion of the otter board with the installation angle.

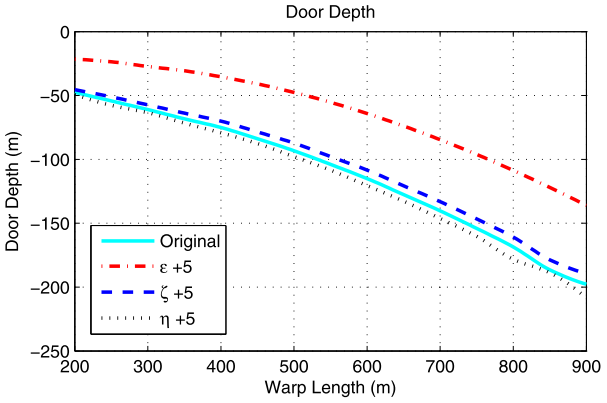


**FIGURE 8.** This figure shows the depth underwater of the otter board with the installation angle.

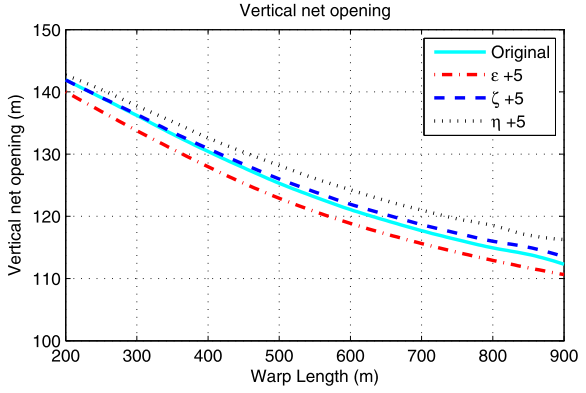


**FIGURE 9.** This figure shows the vertical opening of the trawl net with the installation angle.

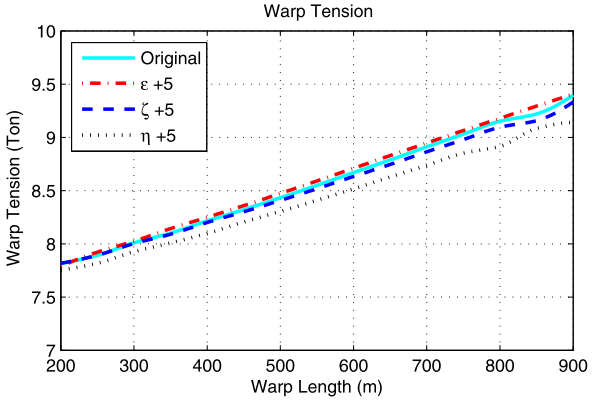


**FIGURE 10.** This figure shows the warp tension with the installation angle.

hand rope are installed in different fixing holes (Fig. 2), different performances are exhibited. In this section, we will analyze the influence of different installation angles of the otter board on the performance of the mid-water trawl system.

When different are used to install the ropes on the otter board, it can be considered that the otter board coordinates rotate around the $\mathbf{x}_m$, $\mathbf{y}_m$, and $\mathbf{z}_m$ axes of the model coordinate by a certain angle. It is assumed that the model coordinate rotates $\varepsilon$, $\zeta$, and $\eta$ angles around its $\mathbf{z}_m$, $\mathbf{y}_m$, $\mathbf{x}_m$ axes, respectively, and can coincide with the otter board coordinate system. The $\varepsilon$, $\zeta$, and $\eta$ angles can be approximated to the variation of the attack angle, the slip angle and the elevation angle of the otter board, respectively. In this paper, the variation angle is chosen to be 5° to study the influence of different otter board mounting angles on the performance of the net. The chosen angle of 5° is generally large enough for the variation of otter board mounting angles.

The simulation results of the mid-water trawl under different otter board installation angles are shown in Fig. 7 ∼ Fig. 12. It can be seen that the $\zeta$ angle has little effect on the simulation results, indicating that the adjustment around the $\boldsymbol{y}_m$ axis is less effective. When using different installation angles, the otter board expansion (Fig. 7) and the vertical expansion of the trawl mouth (Fig. 9) are all between 5% and 10%, and the two have a trade-off relationship. The tendency of the warp tension (Fig. 10) varies with the installation angle and is similar to the otter board expansion

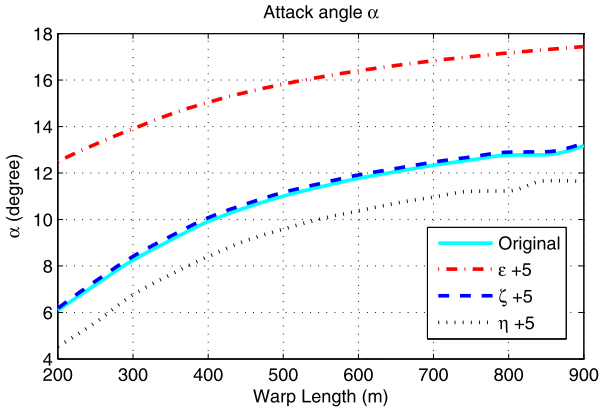


**FIGURE 11.** This figure shows the attack angle of the otter board with the installation angle.

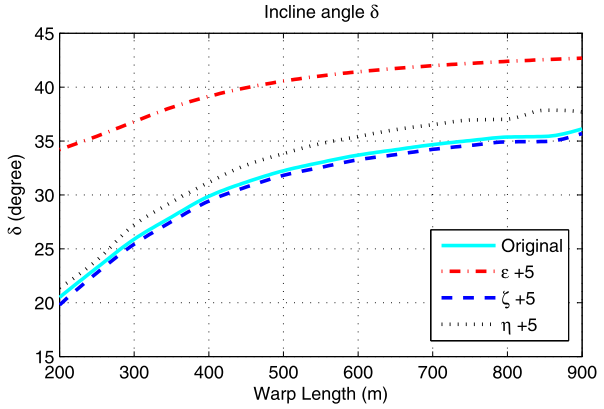


**FIGURE 12.** This figure shows the inclination angle of the otter board with the installation angle.

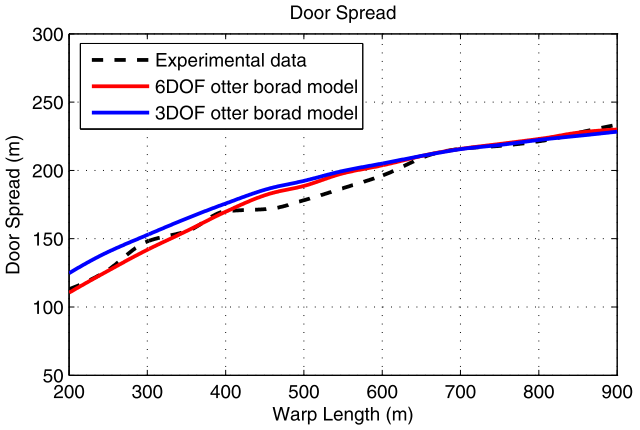


**FIGURE 13.** Comparison of the simulated and sea-trial door spreads with the warp length. The blue and red solid lines are the simulated 6DOF and 3DOF results, respectively, and the black dotted line is the sea-trial results.

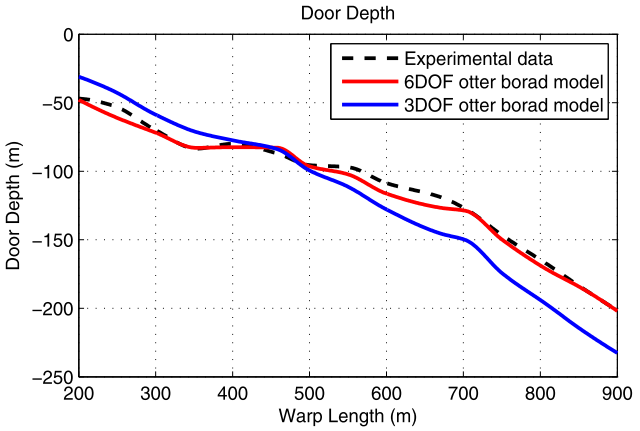


**FIGURE 14.** Comparison of the simulated and sea-trial door depths with the warp length.

(Fig. 7), since the changes in these two values are directly related to the lift change of the otter board.

It can be seen from Fig. 11 that an increase in the $\boldsymbol{\varepsilon}$ angle will lead to an increase in the angle of attack $\alpha$ and the inclination $\delta$ of the otter board, and the increases in $\alpha$ and $\delta$ are above 5°, which is caused by the increase in the angle of attack $\alpha$. The increase in the hydrodynamic $C_x^M$, in turn causes an increase in $\delta$.

As seen in Fig. 12, the increase in the $\eta$ angle will result in a decrease in the attack angle $\alpha$ and an increase in the inclination angle $\delta$, but the changes in both are not large, because the decrease in $\alpha$ reduces the $C_x^M$, and thus the change in the inclination $\delta$ is weakened. It can be seen from the above analysis that an increase in the $\varepsilon$ angle causes an increase in the attack angle $\alpha$ and the inclination angle $\delta$, and both the change in $\alpha$ and the change in $\delta$ cause an increase in the hydrodynamic force in the vertical direction. Therefore, the otter board depth (Fig. 8) is strongly affected by the change in the $\varepsilon$ angle. When the $\varepsilon$ angle is increased by 5°, the depth of the otter board is reduced by approximately 30%.

### *D. SEA-TRIAL VERIFICATION*

Fig. 13 ∼ Fig. 16 show the mid-water trawl comparison between the sea trial and the simulation results including both the 6-DOF and the 3-DOF otter board models. The primary parameters of the 6-DOF model can be found from Eq. (37), and the lift and drag coefficients of the 3-DOF model are obtained by Chen *et al.* [24], in which $\alpha$ and $\beta$ are the average values.

It can be seen from the figures that the simulation results for the 6-DOF otter board model are very close to the results of the sea trial. The simulation errors of the otter board expansion, otter board depth, mesh depth and warp tension are 4.8%, 4.5%, 7.4% and 2.6%, respectively, indicating that the 6-DOF otter board model established in this paper predicts the performance of the trawl net very well.

As seen in Fig. 13 and Fig. 16, the otter board expansion and the warp tension results of the 6-DOF and 3-DOF models are close. The otter board expansion of the 6-DOF model increases slightly faster than that of the 3-DOF model with an increase in warp length (Fig. 13). This is because the increase in $\alpha$ leads to a lift increase in the otter board.

However, the trawl depth and otter board's depth changes with the increase in warp length for the 3-DOF model are significantly faster than those for the 6-DOF model (Fig. 14, Fig. 15). This is primarily due to the increase in inclination

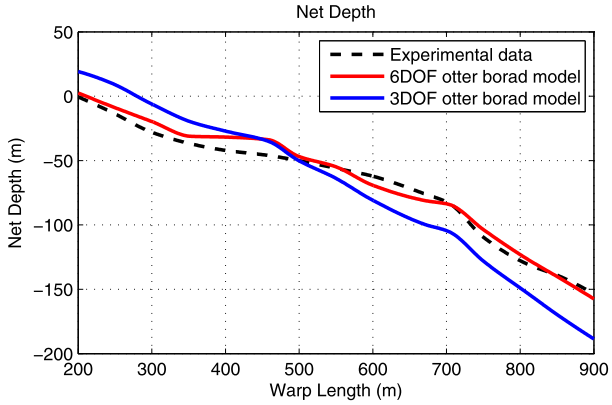


**FIGURE 15.** Comparison of the simulated and sea-trial trawl net depths with the warp length.

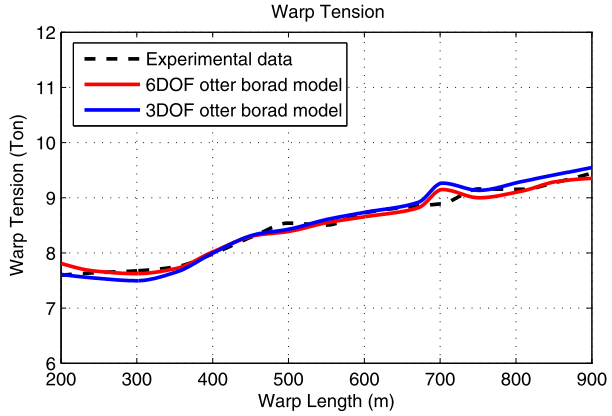


**FIGURE 16.** Comparison of the simulated and sea-trial warp tensions with the warp length.

angle $\delta$ with the increase in warp length, which enables the larger lift force in the vertical direction. When the warp length varies from 200 m to 900 m, the error between the 3-DOF otter board model and the sea test result is approximately 25%, which is much larger than the approximately 5% error in the results with the 6-DOF otter board model. This finding indicates that when the range of the warp length is large, the performance of the trawl net can be calculated more accurately by using the 6-DOF otter board model.

The warp tension can be regarded as a combined force of the horizontal resistance, gravity and the lift force of the trawl. Since the force in the vertical direction in the 6-DOF otter board model is small compared with that in the 3-DOF otter board model, the total tension in the drawing is also small as in Fig. 16.

## V. CONCLUSION

In this paper, a mathematical model of a mid-water trawl system including the towed warp, the trawl net, the otter board and other rigging components was established. The otter board was considered as a 6-DOF model, and the variation of the otter board's hydrodynamic parameters with different yaws, pitches and roll angles was also considered. A first-order approximation was adopted to simplify the relationship between the otter board's hydrodynamic parameters and its working angle, and the coefficients included in the otter board model were then estimated by sea trail data. The influence of the otter board configuration on the performance of the mid-water trawl was analyzed with the simulation results, and a sea-trial was conducted to verify the effectiveness of the proposed mathematical model. The final results of the door depth and the door spread with warp lengths from 200 m ∼ 900 m showed good agreements with the sea trail data, and the mean normalized absolute error between the simulation and the measurement was approximately 5%.

## ACKNOWLEDGMENTS

The authors thank the reviewers for their elaborate and incisive suggestions.

## REFERENCES

[1] J. S. Bessonneau and D. Marichal, "Study of the dynamics of submerged supple nets (applications to trawls)," *Ocean Eng.*, vol. 25, no. 7, pp. 563–583, 1998.
[2] H.-H. Park, "A method for estimating the gear shape of a mid-water trawl," *Ocean Eng.*, vol. 34, nos. 3–4, pp. 470–478, 2007.
[3] J. Prat *et al.*, "A simplified model of the interaction of the trawl warps, the otterboards and netting drag," *Fisheries Res.*, vol. 94, no. 1, pp. 109–117, 2008.
[4] J. H. Lee, L. Karlsen, and C. W. Lee, "A method for improving the dynamic simulation efficiency of underwater flexible structures by implementing non-active points in modelling," *ICES J. Mar. Sci.*, vol. 65, no. 9, pp. 1552–1558, 2008.
[5] Y. Yao, Y. Chen, H. Zhou, and H. Yang, "A method for improving the simulation efficiency of trawl based on simulation stability criterion," *Ocean Eng.*, vol. 117, pp. 63–77, May 2016.
[6] X. Sun, Y. Yin, Y. Jin, X. Zhang, and X. Zhang, "The modeling of single-boat, mid-water trawl systems for fishing simulation," *Fisheries Res.*, vol. 109, no. 1, pp. 7–15, 2011.
[7] L. Chun-Woo, "Depth control of a midwater trawl gear using fuzzy logic," *Fisheries Res.*, vol. 24, no. 4, pp. 311–320, 1995.
[8] C.-W. Lee, J.-H. Lee, and I. J. Kim, "Application of a fuzzy controller to depth control of a midwater trawl net," *Fisheries Sci.*, vol. 66, no. 5, pp. 858–862, 2000.
[9] F. Hu, T. Tokai, K. Matuda, H. Fuxiang, T. Tadashi, and M. Ko, "A computer simulation for the net position control of midwater trawl system," *Nippon Suisan Gakkaishi*, vol. 67, no. 2, pp. 226–230, 2001.
[10] H. Zhou, Y.-L. Chen, and H.-Y. Yang, "Robust optimal output tracking control of a midwater trawl system based on T-S fuzzy nonlinear model," *China Ocean Eng.*, vol. 27, no. 1, pp. 1–16, Mar. 2013.
[11] Y.-L. Chen, H. Zhou, Y.-G. Zhao, and J.-Y. Hou, "Fuzzy robust path tracking strategy of an active pelagic trawl system with coordinated ship and winch regulation," *J. Central South Univ.*, vol. 21, no. 1, pp. 167–179, Jan. 2014.
[12] Z. Chen, Y.-J. Pan, and J. Gu, "Integrated adaptive robust control for multilateral teleoperation systems under arbitrary time delays," *Int. J. Robust Nonlinear Control*, vol. 26, no. 12, pp. 2708–2728, Aug. 2016.
[13] Z. Chen, B. Yao, and Q. Wang, "$\mu$-synthesis-based adaptive robust control of linear motor driven stages with high-frequency dynamics: A case study," *IEEE/ASME Trans. Mechatronics*, vol. 20, no. 3, pp. 1482–1490, Jun. 2015.
[14] M. Yuan, Z. Chen, B. Yao, and X. Zhu, "Time optimal contouring control of industrial biaxial gantry: A high-efficient analytical solution of trajectory planning," *IEEE/ASME Trans. Mechatronics*, vol. 22, no. 1, pp. 247–257, Feb. 2017.
[15] J. Yao and W. Deng, "Active disturbance rejection adaptive control of hydraulic servo systems," *IEEE Trans. Ind. Electron.*, vol. 64, no. 10, pp. 8023–8032, Oct. 2017.
[16] J. Yao, W. Deng, and Z. Jiao, "RISE-based adaptive control of hydraulic systems with asymptotic tracking," *IEEE Trans. Autom. Sci. Eng.*, vol. 14, no. 3, pp. 1524–1531, Jul. 2017.

[17] Z. Chen, B. Yao, and Q. Wang, "Accurate motion control of linear motors with adaptive robust compensation of nonlinear electromagnetic field effect," *IEEE/ASME Trans. Mechatronics*, vol. 18, no. 3, pp. 1122–1129, Jun. 2013.
[18] K. J. Reite and A. J. Sorensen, "Mathematical modeling of the hydrodynamic forces on a trawl door," *IEEE J. Ocean. Eng.*, vol. 31, no. 2, pp. 432–453, Apr. 2006.
[19] F. Mellibovsky, J. Prat, E. Notti, and A. Sala, "Testing otter board hydrodynamic performances in wind tunnel facilities," *Ocean Eng.*, vol. 104, pp. 52–62, Aug. 2015.
[20] X. Shen, F. Hu, T. Kumazawa, D. Shiode, and T. Tokai, "Hydrodynamic characteristics of a hyper-lift otter board with wing-end plates," *Fisheries Sci.*, vol. 81, no. 3, pp. 433–442, 2015.
[21] Y. Takahashi, Y. Fujimori, F. Hu, X. Shen, and N. Kimura, "Design of trawl otter boards using computational fluid dynamics," *Fisheries Res.*, vol. 161, pp. 400–407, Jan. 2015.
[22] L. Leifsson, E. Hermannsson, and S. Koziel, "Optimal shape design of multi-element trawl-doors using local surrogate models," *J. Comput. Sci.*, vol. 10, pp. 55–62, Sep. 2015.
[23] T. Takagi, T. Shimizu, K. Suzuki, T. Hiraishi, and K. Yamamoto, "Validity and layout of 'NaLA': A net configuration and loading analysis system," *Fisheries Res.*, vol. 66, nos. 2–3, pp. 235–243, 2004.
[24] Y. Chen, Y. Zhao, H. Zhou, H. Huang, "Simulation study of large mid-water trawl system," *J. Zhejiang Univ. (Eng. Sci.)*, vol. 48, no. 4, pp. 625–632, 2014.
[25] I. M. Jonsson, L. Leifsson, S. Koziel, Y. A. Tesfahunegn, and A. Bekasiewicz, "Shape optimization of trawl-doors using variable-fidelity models and space mapping," *Procedia Comput. Sci.*, vol. 51, no. 1, pp. 905–913, 2015.
[26] E. Jonsson, S. Koziel, and L. Leifsson, "Computational fluid dynamic analysis and shape optimization of trawl-doors," in *Proc. 51st AIAA Aerosp. Sci. Meeting Including New Horizons Forum Aerosp. Expo.*, 2013, pp. 25–36.
[27] L. Leifsson, S. Koziel, and E. Jonsson, "Hydrodynamic shape optimization of fishing gear trawl-doors," in *Proc. Int. Conf. Simulation Modeling Methodol., Technol. Appl.* Cham, Switzerland: Springer, 2014, pp. 305–318.
[28] Y. Chen, "Research on modeling and control strategies for the trawling system," Ph.D. dissertation, Dept. Mech. Eng., Zhejiang Univ., Hangzhou, China, 2013.

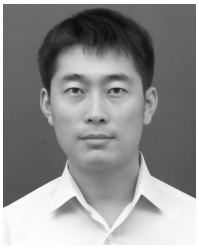

**YINGLONG CHEN** received the B.Eng. and Ph.D. degrees in mechatronic control engineering from Zhejiang University, China, in 2008 and 2013, respectively. From 2013 to 2016, he was a Research Assistant with the School of Mechanical Engineering, Zhejiang University. Since 2017, he has been an Assistant Professor with the Naval Architecture and Ocean Engineering College, Dalian Maritime University. His research interests include fluid power transmission and control, advanced motion control of mechatronic systems, and robotics.

**YEMING YAO** received the B.Eng. degree in mechanical engineering from the Huazhong University of Science and Technology, China, in 2011, and the Ph.D. degree in mechatronic control engineering from Zhejiang University, China, in 2016. Since 2016, he has been an Engineer with the Nanjing Engineering Institute of Aircraft Systems, Jincheng, AVIC. His research interests include fluid power transmission and control and marine engineering equipment.

**ZENGMENG ZHANG** received the B.Eng. and Ph.D. degrees in mechatronic control engineering from Zhejiang University, China, in 2003 and 2009, respectively. Since 2009, he has been a Professor with the Naval Architecture and Ocean Engineering College, Dalian Maritime University. His research interests include fluid power transmission and control, water hydraulics, and artificial muscles.

**HUA ZHOU** received the B.Eng., M.Eng., and Ph.D. degrees in mechanical engineering from the Central China University of Science and Engineering, China, in 1990, 1993, and 1997, respectively. Since 2000, he has been a Professor with the Mechanical Engineering College, Zhejiang University. His research interests include fluid power transmission and control, water hydraulics, and electro-hydraulic proportional control system.